Applied Physics B (2022) 128: 190
https://doi.org/10.1007/s00340-022-07913-9

Applied Physics B
Lasers and Optics

RESEARCH

Switchable L-band dual-wavelength dark–bright pulse pair generation from an Er-doped mode-locked fiber laser with SMF–GIMF–SMF as the saturable absorber

Mengyuan Liu[1,2] · Yaoyao Qi[1,2] · Song Yang[3] · Zhenxu Bai[1,2] · Bingzheng Yan[1,2] · Jie Ding[1,2] · Yulei Wang[1,2] · Zhiwei Lu[1,2]

Received: 14 July 2022 / Accepted: 20 September 2022 / Published online: 26 September 2022

Abstract
We have demonstrated the dual-wavelength domain-wall pulse operation in an Er-doped mode-locked fiber laser based on single-mode fiber (SMF)–graded index multimode fiber (GIMF)–SMF as the saturable absorber for the first time. The domain-wall dark–bright pulse pairs exhibited two peaks, which were located at 1604.6 and 1606 nm. The pulse repetition rate was maintained at 16.5 MHz throughout the dark–bright pulse pairs operation. Besides, dark–bright pulse pairs operation was demonstrated at a relative stability with the signal to noise ratio of 55.3 dB. Moreover, the dark–bright pulse pairs could be converted into bright–dark pulse pairs by adjusting the polarization state, which has potential advantages for the development of wavelength division multiplexing and optical fiber sensing technology.

1 Introduction

Soliton formation is a topic that has attracted an extensive investigation in recent years due to its many potential applications, such as optical communications [1], ultra-precision manufacturing [2], and bio-medicine [3]. To date, most of the reported works on soliton mode-locked lasers are operating under the bright pulse regime [4–6]. Besides bright pulses, the so-called dark solitons that are also solutions of the nonlinear Schrödinger equation (NLSE) [7]. These solitons are also further identified as solutions of the complex Ginzburg–Landau equation (CGLE) [8]. Here, dark solitons are referred to as a train of intensity dips in a continuous wave (CW) background of the laser emission [9]. Comparing with bright solitons, dark pulses have better stability in the presence of noise [10], being less influenced by intrapulse stimulated Raman scattering (ISRS) [11], which is due to the ISRS can cause a shift of dark solitons, the rate of the shift is half the corresponding value for bright solitons if the slow loss of contrast is neglected. These characteristics make dark pulses having potential applications in optical communications.

The formation of dark pulses can be classified into three mechanisms, which are NLSE dark pulse [12], cubic–quintic nonlinear Schrödinger equation (CQNLSE) dark pulse [13] and domain-wall (DW) dark pulse [14], which can also be called domain-wall solitons (DWSs) [15]. Especially for the DWSs operated in both normal dispersion and anomalous

✉ Yaoyao Qi
qiyao@hebut.edu.cn

Mengyuan Liu
meng13292259057@163.com

Song Yang
sonya@dtu.dk

Zhenxu Bai
zxbai@hebut.edu.cn

Bingzheng Yan
yanbz1994@foxmail.com

Jie Ding
dingj1993@126.com

Yulei Wang
wyl@hebut.edu.cn

Zhiwei Lu
zhiweilv@hebut.edu.cn

[1] Center for Advanced Laser Technology, School of Electronics and Information Engineering, Hebei University of Technology, Tianjin 300401, China

[2] Hebei Key Laboratory of Advanced Laser Technology and Equipment, Tianjin 300401, China

[3] DTU Fotonik, Department of Photonics Engineering, Technical University of Denmark, 2800 Kgs. Lyngby, Denmark

dispersion cavity, they are usually based on two or more lasing at different wavelengths oscillating, which have attracted intense interest in optical communication and optical signal processing systems in the past recent years [16]. In 2015, Z C Tiu et al. have demonstrated NLSE dark pulse [17], switchable DW dark pulse and CQNLSE dark pulse based on nonlinear polarization rotation (NPR) technique [13]. Furthermore, dark pulse generation has also been demonstrated using different saturable absorbers (SAs), such as black phosphorus and glycerin [18, 19]. In addition, due to the interaction between solitons, there also exist bright–dark, or dark–bright pulse pairs when they propagate together in the medium, which has been theoretically demonstrated by using the NLSE [20] and have been realized experimentally in passively mode-locked fiber lasers based on nonlinear amplifying loop mirror (NALM) [21] and NPR [22]. Subsequently, in 2016, B Guo et al. used topological insulator: Bi_2Se_3 as an SA to obtain bright–dark soliton pairs in an Er-doped fiber laser. They have demonstrated that bright and dark soliton pairs are orthogonal polarizations [23]. In 2018, R W Zhao et al. observed for the first time three-wavelength dark–bright pulse pair operation based on ReS_2 [24]. Recently, dual-wavelength bright–dark soliton pairs have also been observed in a fiber laser based on $ZrSe_2$ [25]. In view of the previous research on dark–bright or bright–dark soliton pairs operation, most of them were realized by low-dimensional materials-based SAs. But, in contrast with material SAs, the GIMF SA possesses many advantages, such as low cost, wide wavelength-tunable output [26], high damage threshold [27], long-term stability, the capability of controllable modulation depth [28]. More importantly, if the length of GIMF is chosen to be hundreds of times larger than the self-imaging period in GIMF, then a larger interaction length can contribute to a higher level of nonlinear effect [29], which is beneficial to the formation of stable domain-wall (a localized nonlinear structure) [30]. However, dark–bright or bright–dark soliton pairs operation in an Er-doped fiber laser based on SMF–GIMF–SMF as the SA have not been reported [31]. Moreover, it is also interesting to analyze the evolution and interconversion of dark–bright or bright–dark soliton pairs in the GIMF mode-locked fiber lasers.

In this manuscript, to the best of our knowledge, we have demonstrated the L-band dual-wavelength DW dark–bright pulse pairs operation in a mode-locked fiber laser based on SMF–GIMF–SMF for the first time. The central wavelengths are 1604.6 and 1606 nm, respectively. Besides, the dark–bright pulse pair has high stability, and the SNR is 55.3 dB, which also confirm that dark solitons have better stability in the presence of noise. At the same time, we experimentally demonstrated that the strong coupling between two different wavelength beams in the fiber laser can result in the formation of DWSs. Moreover, the dark–bright pulse pairs could be converted into bright–dark pulse pairs by carefully adjusting the polarization state. The dark–bright or bright–dark pulse pair train can be generated on two wavelengths, which is important for developing the wavelength division multiplexing and optical fiber sensing technology [32].

1.1 The characteristics of the GIMF-based SA

The GIMF-based SA consists of a segment GIMF (62.5/125 μm) spliced at both ends to two standard SMFs, as illustrated in Fig. 1. The saturable absorption effect results from the nonlinear multimode interference (NL–MMI) in the GIMF, which is the interference of excited modes in a multimode optical fiber when single-mode light is coupled to a multimode optical fiber which results in a periodic interference pattern along the fiber. This is the so-called self-imaging. It takes place when the input field is replicated after traveling some distance in the direction of propagation in the GIMF. In the nonlinear regime where the peak power is high, self-phase modulation (SPM) and cross-phase modulation (XPM) effects both influence the propagation constant of every mode and hence change the self-imaging length of the light in the GIMF. Therefore, the self-imaging length of the pulse wing is different from its peak [33]. For the low-power light (the yellow line in Fig. 1), the light beam expands and experiences a large loss owing to the core diameter mismatch between GIMF and SMF. While for the high-power light (the red line in Fig. 1), self-focusing effect occurs and the light power coupled into the core of SMF is maintained. Therefore, as long as we accurately control the length of the multimode fiber, the high-power light in the multimode fiber can be coupled to the next section of SMF at low loss, while low-power light experiences large loss, and the effect of SA can be achieved.

In order to determine the most appropriate length of GIMF, the numerical simulation of the SMF–GIMF–SMF SA was built by Rsoft. Figure 2a shows the mode distribution of the SA along the propagation direction. The periodic power fluctuation in Fig. 2b indicates that the self-imaging points were formed in the propagation direction, and the peaks were the positions of the self-imaging points. In addition, we also recorded the transverse light field distribution of the SMF–GIMF–SMF when $Z = 0$,

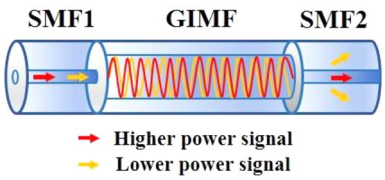

Fig. 1 Schematic structure of SMF–GIMF–SMF

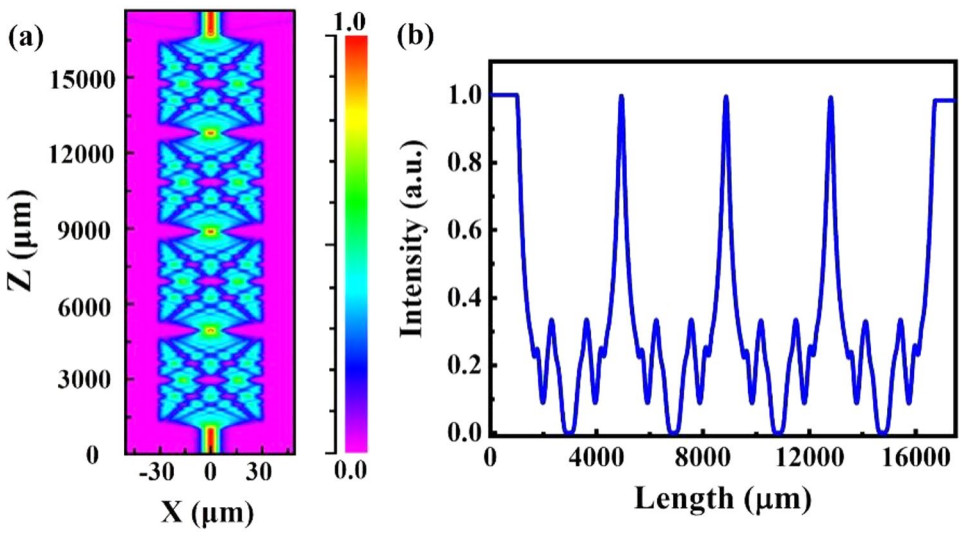

Fig. 2 The mode distribution and the intensity distribution of the SMF–GIMF–SMF. **a** Mode distribution of the SMF–GIMF–SMF; **b** Intensity distribution of the SMF–GIMF–SMF

1000, 2000, 3000, 4000, 4900 μm. It can be seen from the Fig. 3, the distribution of interference light field in GIMF also changes with the change of transmission distance. When $Z=0$ μm, it is the field intensity distribution when the beam enters the GIMF from the SMF, and the self-image effect occurs at $Z=4900$ μm. Therefore, we can confirm that the

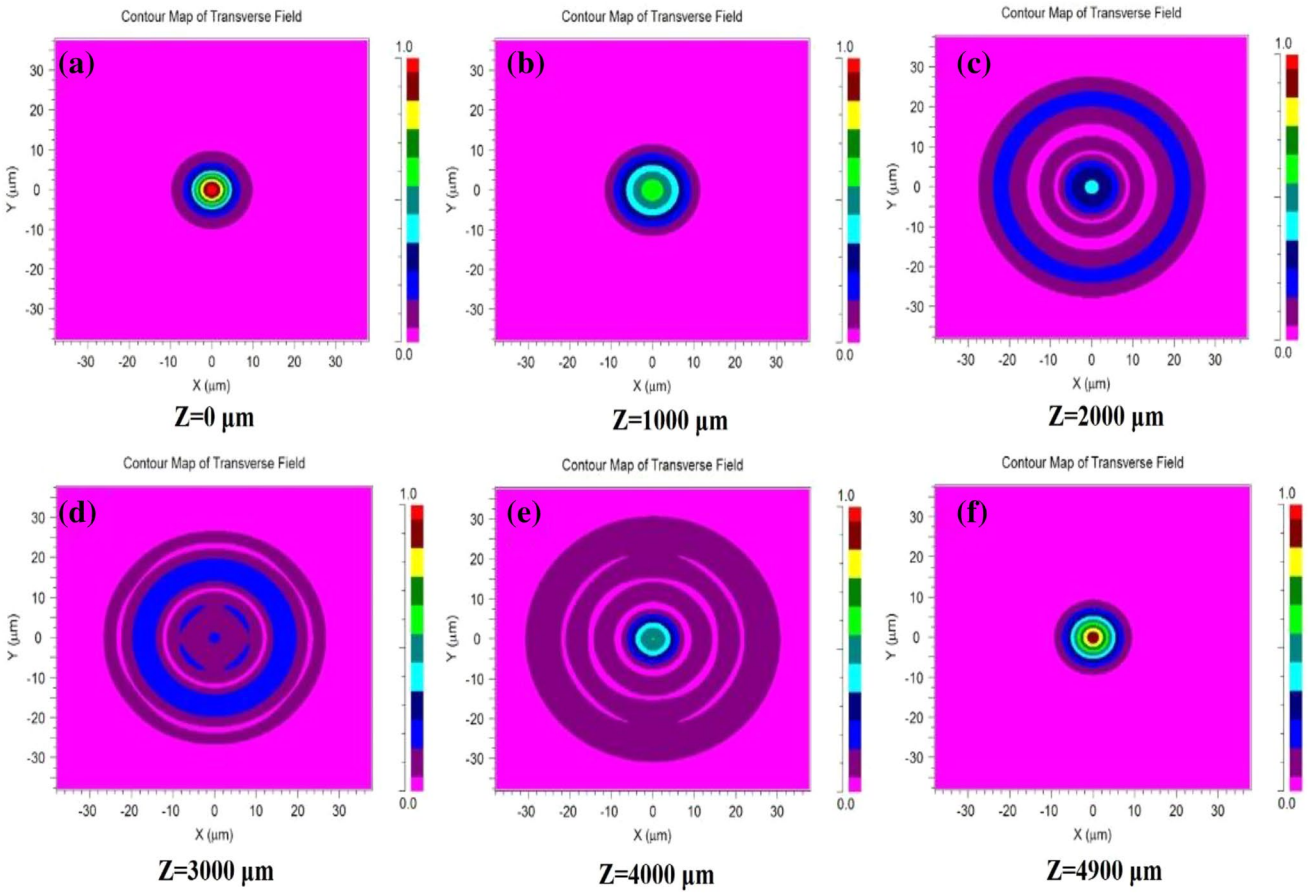

Fig. 3 Transverse light field distribution of SMF–GIMF–SMF: **a** $Z=0$ μm; **b** $Z=1000$ μm; **c** $Z=2000$ μm; **d** $Z=3000$ μm; **e** $Z=4000$ μm; **f** $Z=4900$ μm

self-imaging period is about 0.39 cm. But, for the convenience of operation, the GIMF of 39 cm was adopted, which is about ~100 times of self-imaging period.

Subsequently, we measured the saturable absorption of the SMF–GIMF–SMF using a high peak power fiber laser centered at 1550 nm. The data obtained from the experiment were then fitted according to:

$$T = 1 - \alpha_{ns} - \frac{\Delta T}{1 + I/I_{sat}}, \quad (1)$$

where α_{ns} is the non-saturable loss, ΔT and I_{sat} are the modulation depth and saturation intensity, respectively. Figure 4 shows the nonlinear transmission curve of the GIMF SA, indicating that the GIMF SA has the modulation depth of 7.7%, the corresponding non-saturable loss is 34.3%. Compared with the reported SMF–GIMF–SMF [29, 34], we only focused on the vector characteristics of the mode-locked pulses based on the SMF–GIMF–SMF SA. In addition, as far as I know, by increasing the input light power until it is higher than the power threshold of reverse saturable absorption effect of GIMF SA, the SA can be changed into the reverse saturable absorption region, and the dissipative soliton resonance (DSR) phenomenon occurs, which has been reported [35]. But, limited by the peak power of our fiber laser, as shown in Fig. 4, we did not observe the reverse saturable absorption features, and the experiment did not generate DSR. Through the above analysis, if we can continue to increase the input light power, the GIMF SA can be changed into the reverse saturable absorption region.

In addition, in order to verify that the SMF–GIMF–SMF has filtering effect. The intensity distributions of different incident wavelengths (1350, 1450, 1550 and 1650 nm) in the transmission direction of GIMF were simulated when the length of GIMF was fixed. As shown in Fig. 5, when the wavelength of the incident light changes from 1350 to 1650 nm, the self-imaging period gradually decreases,

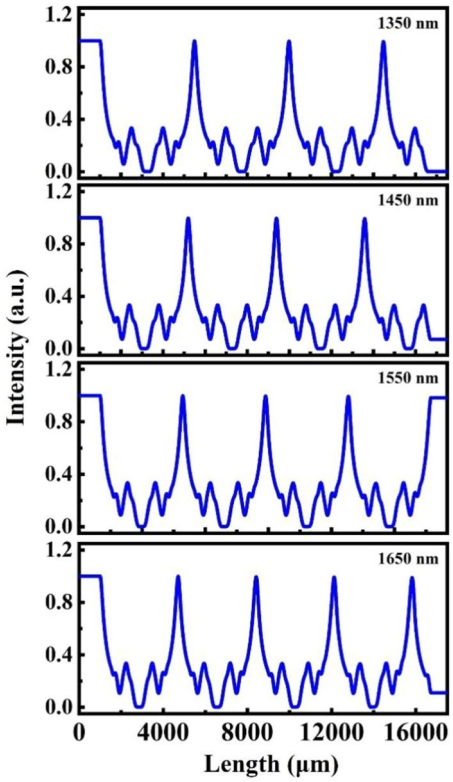

Fig. 5 The intensity distribution of different incident wavelength in GIMF transmission direction

making the position of the self-imaging point different. Therefore, the light energy incident from the GIMF to the SMF is also different, and the coupling ratio changes. In other words, when a broadband source passes through a fixed-length SMF–GIMF–SMF structure, only most of the specific wavelengths of light will be transmitted, and other wavelengths of light will suffer different losses. So, adding the SMF–GIMF–SMF structure in the fiber laser can achieve good filtering effect. Furthermore, as shown in Fig. 6, the transmission spectrum of the SMF–GIMF–SMF in a spectral

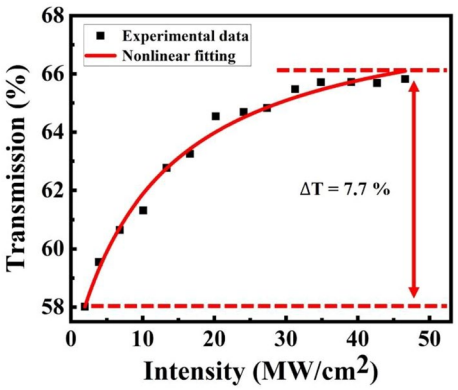

Fig. 4 The nonlinear transmission curve of SMF–GIMF–SMF

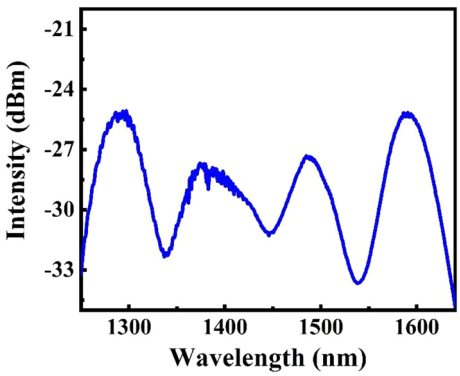

Fig. 6 Transmission spectrum of the SMF–GIMF–SMF

range from 1250 to 1640 nm was tested by an optical spectrum analyzer (OSA) and a broadband light source, which also confirmed that the structure has an obvious filter effect.

2 Experimental setup

Figure 7 shows the schematic diagram of the proposed mode-locked Er-doped fiber laser with a ring cavity configuration based on the SMF–GIMF–SMF device. The 976 nm pump laser diode (LD) with a maximum power of 637 mW is coupled into the laser cavity via a 980/1550 nm wavelength division multiplexer (WDM). A 3 m Er-doped fiber (EDF) (Nufern, SM-ESF-7/125) is used as the gain medium, which is then connected to the SMF–GIMF–SMF device and subsequently to the polarization controller (PC)1 and a polarization insensitive isolator (PI-ISO). The SMF–GIMF–SMF device acts as the mode-locker of the system. The PC1 employed to optimize the mode-locking operation as well as the intracavity birefringence, and the PI-ISO ensures the unidirectional propagation of the laser in the cavity. Subsequently the 10% portion of a 90:10 fused coupler provides the laser output while the 90% portion is engaged to feedback into the cavity. Outside the cavity, a polarization beam splitter (PBS) is applied to separate the orthogonal polarized dark–bright pulse pair. The PC2 located before the external PBS is used to balance the linear polarization change caused by the lead fibers used outside of the cavity and find two Eigen linear polarization states of the laser emission. The total length of the entire cavity is 12.3 m; thus, the round-trip dispersion of the whole cavity is – 0.03 ps^2 (including 3 m EDF with dispersion of – 46.25 ps/nm/km and 8.9 m SMF with dispersion of 18 ps/nm/km). The laser performance is observed using an OSA (Yokogawa, AQ6370D) with 0.02 nm resolution, 1 GHz digital oscilloscope (Tektronix, TDS 5104B) together with a 5 GHz photon detector (Thorlabs DET08CFC/M).

3 Experimental results and discussion

3.1 Generation of dual-wavelength DWSs

In our experiment, the dependence of output power on the pump power for the fiber laser was firstly studied, as shown in Fig. 8. When the pump power is below the mode-locking threshold of 120 mW, only CW operation happens. As long as the pump power can be increased above the mode-locking threshold, the dark–bright pulse pairs emission can be observed. But limited by the maximum pump power of 637 mW, the maximum output power of the mode-locked fiber laser is 18.5 mW. The low efficiency may be caused by the large loss of connection and transmission in the cavity. In future research, the parameters of the resonator will be further optimized, which are expected to improve the laser efficiency.

Figure 9a presents the typical dark–bright pulse pairs operation at the pumping power of 415 mW. The output power of the pulse train is 10.9 mW, and the interval of the pulse train is 60.6 ns, corresponding to the fundamental cavity frequency of 16.5 MHz. Limited by the bandwidth of

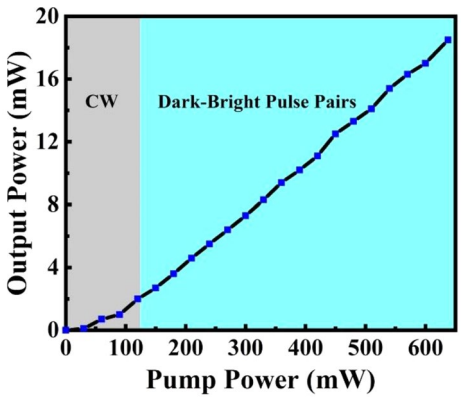

Fig. 8 The laser output power versus the pump power

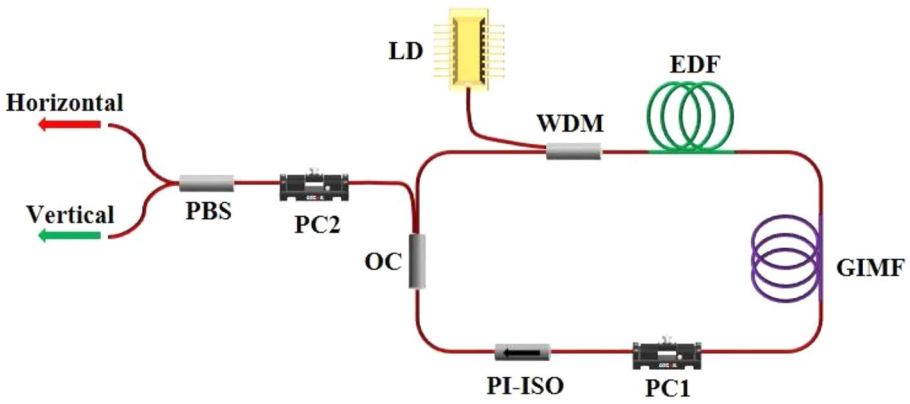

Fig. 7 Schematic of the Er-doped fiber (EDF) ring laser. *WDM* wavelength division multiplexer, *EDF* erbium-doped fiber, *GIMF* grade index multimode fiber, *PC* polarization controller, *PI-ISO* polarization-independent isolator, *OC* optical coupler, *PBS* polarization beam splitter

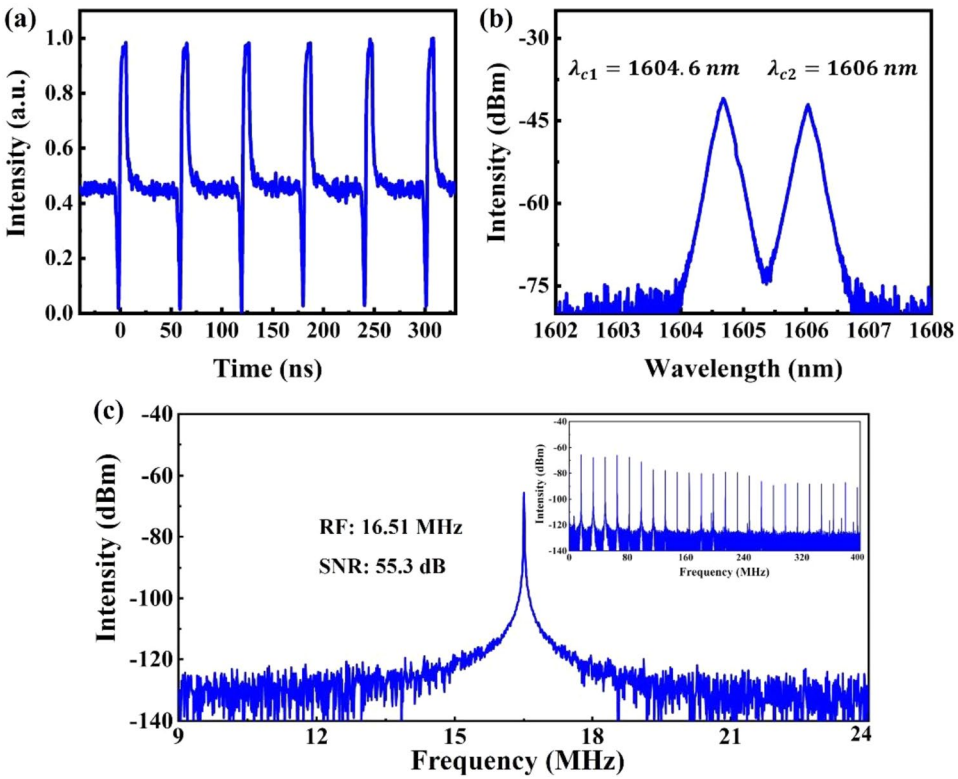

Fig. 9 Mode locked emission at 415 mW of pumping power. **a** Oscilloscope trace; **b** Optical spectrum, and **c** RF spectrum trace, (inset: the RF spectrum trace with 400 MHz span)

oscilloscope, the pulse width of the bright and dark pulse could not be accurately measured, but the depth of the dark pulse is nearly equal to the intensity of the bright pulse in uniform CW background. This phenomenon attributed to the gain of the cavity and the nonlinear effect [36, 37]. Due to the net cavity dispersion of the fiber laser is – 0.03 ps^2, the mechanism of the dark–bright pulse train generated by the fiber laser can be explained by the DWSs theory, two lasing beams originated from two Eigen operation states of fiber lasers are coupled incoherently with each other [38]. That is, due to the existence of fiber birefringence, fiber can support two orthogonal degenerate modes. If the laser cavity does not include a polarization dependent device, the effect of cross-coupling between the two orthogonal polarization light components will induce the formation of stable localized nonlinear structures [19]. In addition, since the GIMF SA has a high level of nonlinear effect, which also promotes cross-coupling of the two orthogonal polarization components [29]. The dual-wavelength spectrum shown in Fig. 9b also confirms this theory, which features of 1604.6 and 1606 nm center wavelength. The generation of dual-wavelength is attributed to the fact that the SMF–GIMF–SMF not only acts as a SA, but also as a filter, which has been simulated, and experimentally demonstrated in various types of fiber lasers [39, 40]. However, it can be seen from Fig. 6 that the bandwidth of the SMF–GIMF–SMF is larger than the spacing of dual-wavelength, which is due to the birefringence induced filtering effect also plays a role in the formation mechanism of dual-wavelength, which has been confirmed in previous works [41]. In addition, the measured radio frequency (RF) spectrum in Fig. 9c shows that the signal to noise ratio (SNR) is 55.3 dB, suggesting relative stability of the mode-locking operation. And, more importantly, the inset in Fig. 9c shows the RF spectrum in a 400 MHz span, which indicates even though there are two operating wavelengths in the cavity, only a single frequency component is observed, which confirms a typical DWS operation whereby the mutual coupling of two wavelengths generates a single frequency component [16]. Meanwhile, when the pump power was 415 mW, a long-term stability examination of the Er-doped mode-locked fiber laser under the laboratory condition has been conducted. Figure 10 shows the measurement results over 48 h. It can be seen from the figure that the relative output power fluctuation is estimated to be less than 5%.

To further investigate polarization characteristics of the dark–bright pulse pairs, a fiber pigtailed external cavity PBS was utilized, so that the two orthogonal principal-polarization components of the output pulses could be measured simultaneously. From Fig. 11a and c, it clearly shows that along two polarization axes, the laser emits different pulse trains, and the average power is 5.1 and 5.7 mW, respectively. Each of the two pulse trains owns the same period of 60.6 ns, corresponding to the fundamental cavity frequency. And the corresponding optical spectra are shown in Fig. 11b and d. We can see that the

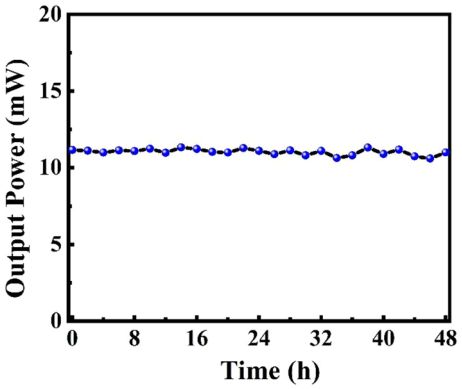

Fig. 10 Power stability of the mode-locked pulses for 48 h

laser emissions along the two orthogonal polarization directions have obvious different central wavelengths of 1604.6 and 1606 nm, showing that the coupling between the two polarization components is incoherent [42].

To give more insight into the dual-wavelength DWSs, we further increased the pumping power with fixed PCs setting. The optical spectra under different pump powers are shown in Fig. 12. The optical spectrum is still dual-wavelength, but the intensity increases gradually, which is similar to the previous report [43].

3.2 Evolution of dual-wavelength DWSs

At a fixed pump power of 415 mW, the pulse durations and the interval between two domain walls could be changed with the variation of the polarization state. Since the total output is the combination of two domain walls, the output pulse shape can also be tuned [29]. As shown in Figs. 13–14, different types of dual-wavelength DWSs operation are observed. Figure 13 shows another type of dark–bright pulse pairs, the pulse width of the bright pulse is in the order of ns, and the two orthogonal polarization components have different central wavelengths of 1603.4 and 1606 nm, respectively.

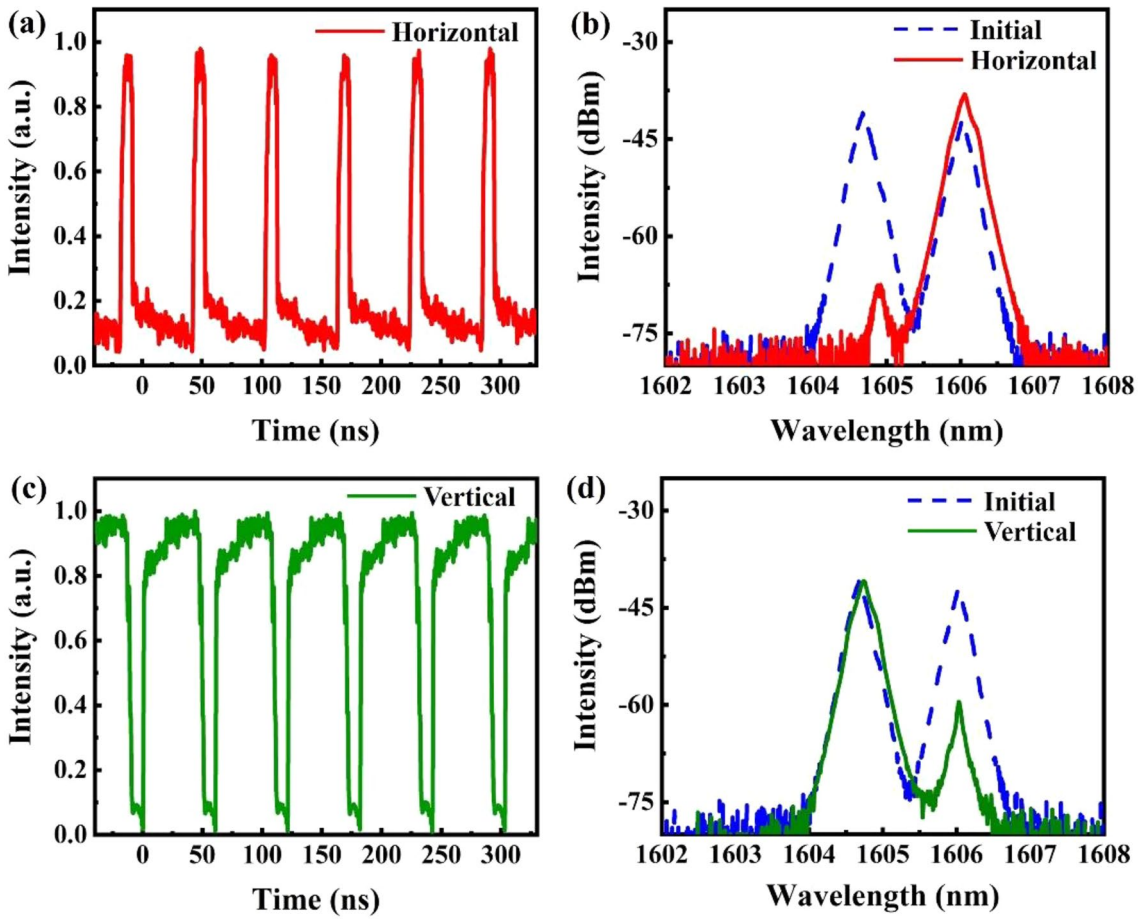

Fig. 11 Separation of the output pulses by PBS. **a** horizontal port. **c** vertical port. **b** and **d** are pulse spectra: the blue line spectrum is measured without PBS; the red and the green lines are the horizontal and vertical port of two orthogonal polarization components resolved with PBS

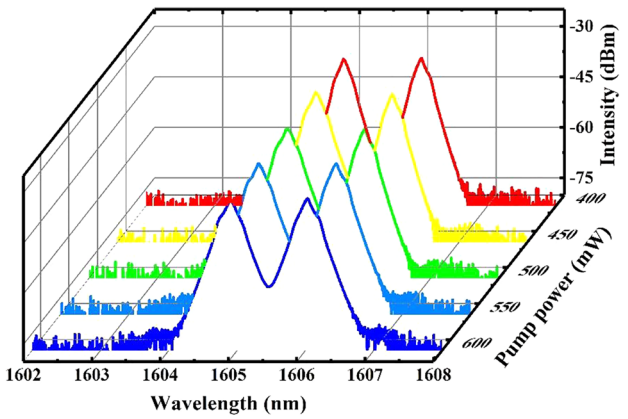

Fig. 12 Spectral distribution of dark–bright pulse pairs under different pump power

In Fig. 14, by further carefully adjusting the PC settings at the same pumping power of 415 mW, another kind of dual-wavelength DWSs, namely bright–dark pulse pairs are obtained through the incoherent coupling between the orthogonal polarization components. Same as the dark–bright pulse train, the adjacent pulse interval is 60.6 ns, corresponding to the fundamental repetition rate of 16.5 MHz. However, due to the evolution of the mode-locking state, the optical spectrum has also changed. The central wavelengths of the two orthogonal polarization components are 1604.8 and 1605.9 nm, respectively.

3.3 Evolution analysis of dark–bright pulse pairs operation

As can be seen from the above experimental results, due to the evolution of the mode-locking state, the optical spectrum has also changed. The outputs can achieve changes in wavelength interval. And the dual-wavelength intervals under different mode-locking states are different, which results from the cavity filtering effect.

Here, we introduce some equations in order to illustrate the basic principles of the SMF–GIMF–SMF structure as a filter with tunable ability. The functional filter effect of the GIMF-based SA originates from the optical interaction between the various modes. The transmission intensity I of a sandwiched-structure SMF-MMF-SMF device with the MMF length of L can be written as followed [44, 45]:

$$I = \sum_{i=1}^{n} I_i + \sum_{i=1}^{n-1} \sum_{j=j+1}^{n} 2\sqrt{I_i I_j}\cos\left(\frac{2\pi\left(n_i - n_j\right)L}{\lambda}\right) \tag{2}$$

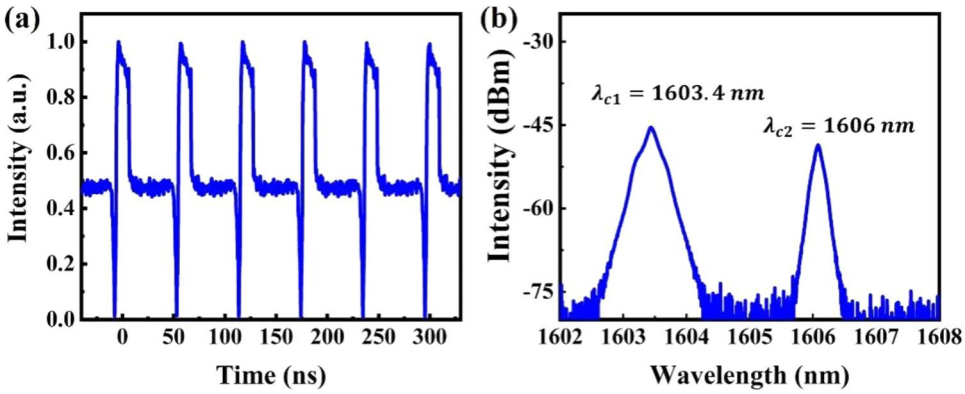

Fig. 13 Dark–bright soliton emission. **a** Oscilloscope trace; **b** Optical spectrum

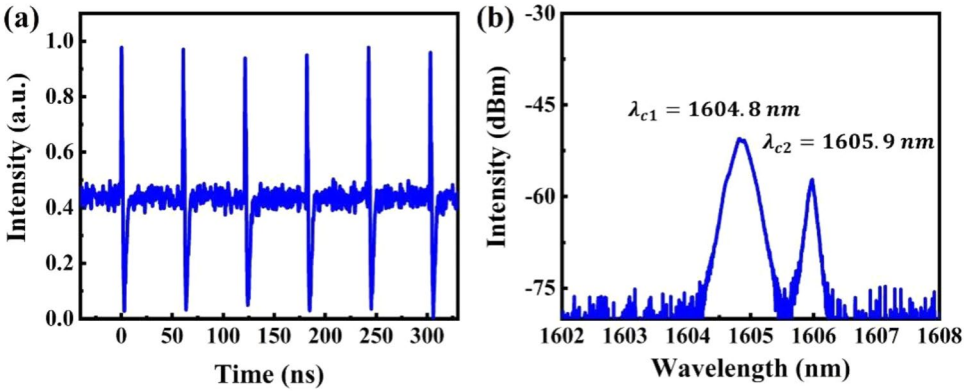

Fig. 14 Bright–dark soliton emission. **a** Oscilloscope trace; **b** Optical spectrum

where I_i and n_i mean the intensity distribution and the corresponding refractive index of the ith-order modes, I_j and n_j are the intensity distribution and the corresponding refractive index of the jth-order modes, L is the length of the GIMF, λ means the operating wavelength. The constructive interference condition of phase matching for two different modes can be given as followed:

$$(n_i - n_j)L = m\lambda_i. \tag{3}$$

The periodic interference pattern of this all-fiber filter originates from the superposition of all interference terms of the various modes. However, the different modes propagating along the GIMF is susceptible to the birefringence intensity induced by changing the polarization state in the intracavity, which can introduce an additional phase shift and change the spectral interval. In addition, due to the birefringence induced filtering effect also plays a role in the formation mechanism of dual-wavelength, which can result in the spacing of dual-wavelength being smaller than the bandwidth of SMF–GIMF–SMF [41].

As can be seen from the above introduction, the SMF–GIMF–SMF not only acts as a SA, but also as a filter, which together with the birefringence induced filtering effect is conducive to the generation of dual-wavelength spectrum. The shape and interval of the dual-wavelength spectrum can be changed by changing the polarization state. In addition, due to the existence of fiber birefringence, fiber can support two orthogonal degenerate modes. Cross-coupling between the two orthogonal polarization light components induces the formation of stable localized nonlinear structures which separate proximal domains of the two orthogonal polarization states of the optical field [42]. Thus, the incoherently coupled DWSs can be obtained by combining the above two effects. The two orthogonal polarization components corresponding to different wavelength distribution. More importantly, since the total output is the combination of two domain walls, the change of dual-wavelength spectrum will make the output pulse shape tunable under the action of SMF–GIMF–SMF filter. Therefore, dark–bright and bright–dark pulse pairs with different spectral structures can be obtained.

4 Conclusion

In conclusion, to the best of our knowledge, we report the experimental observation of the dual-wavelength DWSs phenomenon in an Er-doped mode-locked fiber laser based on SMF–GIMF–SMF SA for the first time. The laser cavity had a compact, simple and all-fiber configuration without any special devices. We firstly demonstrated the generation of dual-wavelength dark-bright pulse pairs experimentally, which were located at 1604.6 and 1606 nm. Besides, the pulse repetition rate was maintained at 16.5 MHz, and the SNR was 55.3 dB. The pulse pairs can be separated into different pulse trains along two polarization axes, which correspond to different wavelengths with orthogonal polarization. In other words, the strong coupling between two different wavelength beams in the fiber laser can result in the formation of DWSs. Besides, the evolution of dark–bright pulse pairs was studied. By adjusting the polarization controllers carefully, we can achieve the interconversion of dark–bright pulse pairs and bright–dark pulse pairs and the tunableness of wavelength interval in our fiber laser. We hope the propagation and evolution mechanism of the dark–bright pulse pair will be well discussed through simulations in the future research.

Author contributions ML: Software, Data curation, Writing - original draft. YQ: Conceptualization, Methodology. SY: Visualization. ZB: Investigation. BY, JD, YW and ZL: Writing - review & editing. All authors reviewed the manuscript.

Funding National Natural Science Foundation of China, 61905065, 61927815.

Declarations

Conflict of interest The authors declare no conflict of interest.

References

1. Y. Zhao, P.L. Guo, X.H. Li, Z.W. Jin, Ultrafast photonics application of graphdiyne in optical communication region. Carbon **149**(11), 336–341 (2019)
2. J.Y. Huang, S. Yang, Investigation on anisotropic tribological properties of superhydrophobic/superlipophilic lead bronze surface textured by femtosecond laser. Appl. Surf. Sci. **579**(3), 152223 (2021)
3. Y.Y. Qi, S. Yang, J.J. Wang, L. Li, Z.X. Bai, Y.L. Wang, Z.W. Lv, Recent advance of emerging low-dimensional materials for vector soliton generation in fiber lasers. Mater. Today Phys. **23**(25), 100622 (2022)
4. R.D. Lv, Y.G. Wang, J. Wang, W. Ren, L. Li, S.C. Liu, Z.D. Chen, Y.F. Li, H.Y. Wang, F.X. Fu, Soliton and bound-state soliton mode-locked fiber laser based on a MoS_2/fluorine mica Langmuir-Blodgett film saturable absorber. Photon. Res. **7**(4), 431–436 (2019)
5. J. Zheng, S. Yang, Z. Zhu, K. Lau, L. Li, Low mode-locking threshold and sub-90 fs Er-doped Mamyshev oscillator. Opt. Commun. **508**, 127711 (2022)
6. Y.J. Zhu, Z.K. Cui, X.G. Sun, T. Shirahata, L. Jin, S. Yamashita, S.Y. Set, Fiber-based dynamically tunable Lyot filter for dual-wavelength and tunable single-wavelength mode-locking of fiber lasers. Opt. Express **28**(19), 27250–27257 (2020)
7. V.E. Zakharov, A.B. Shabat, Interaction between solitons in a stable medium. J. Exp. Theor. Phys. **37**(5), 823–828 (1973)

8. W.V. Saarloos, P.C. Hohenberg, Fronts, pulses, sources and sinks in generalized complex Ginzburg-Landau equations. Physica D **56**(4), 303–367 (1992)
9. S. Yang, Q. Zhang, Z. Zhu, P. Yin, Y. Ge, L. Li, L. Jin, L. Zhang, H. Zhang, Recent advances and challenges on dark solitons in fiber lasers. Opt. Laser Technol. **152**, 108116 (2022)
10. Y.C. Meng, S.M. Zhang, H.F. Li, J. Du, Y.P. Hao, X.L. Li, Bright-dark soliton pairs in a self-mode locking fiber laser. Opt. Eng. **51**(6), 064302 (2012)
11. W. Zhao, E. Bourkoff, Generation, propagation, and amplification of dark solitons. J. Opt. Soc. Am. B **9**(7), 1134–1144 (1992)
12. D.Y. Tang, L. Li, Y.F. Song, L.M. Zhao, H. Zhang, D.Y. Shen, Evidence of dark solitons in all-normal-dispersion-fiber lasers. Phys. Rev. A **88**(1), 18592–18601 (2013)
13. Z.C. Tiu, M. Suthaskumar, A. Zarei, S.J. Tan, H. Ahmad, S.W. Harun, Generation of switchable domain wall and cubic-quintic nonlinear Schrödinger equation dark pulse. Opt. Laser Technol. **73**, 127–129 (2015)
14. H. Zhang, D.Y. Tang, L.M. Zhao, R.J. Knize, Vector dark domain wall solitons in a fiber ring laser. Opt. Express **18**(5), 4428–4433 (2010)
15. P. Wang, K.J. Zhao, X.S. Xiao, C.G. Yang, Pulse dynamics of dual-wavelength dissipative solition resonances and domain wall solitions in a Tm fiber laser with fiber-based Lyot filter. Opt. Express **25**(24), 30708–30719 (2017)
16. H. Ahmad, Z.C. Tiu, A. Zarei, M. Suthaskumar, M.A.M. Salim, S.W. Harun, Domain-wall dark pulse generation in fiber laser incorporating MoS_2. Appl. Phys. B (2016). https://doi.org/10.1007/s00340-016-6343-x
17. Z.C. Tiu, A. Zarei, S.J. Tan, H. Ahmad, S.W. Harun, Harmonic dark pulse emission in Erbium-doped fiber laser. Chin. Phys. Lett. **32**(3), 034203 (2015)
18. J.Y. Liu, F.Y. Zhao, H.S. Wang, W. Zhang, X.H. Hu, X.H. Li, Y.S. Wang, Generation of dark solitons in erbium-doped fiber laser based on black phosphorus nanoparticles. Opt. Mater. **89**(4), 100–105 (2019)
19. W.Y. Zhang, L. Zhan, T.H. Xian, L.R. Gao, Generation of bright/dark pulses in an Erbium-doped fiber laser mode-locked with glycerin. J. Lightwave Technol. **37**(15), 3756–3760 (2019)
20. R. Radhakrishnan, K. Aravinthan, A dark-bright optical soliton solution to the coupled nonlinear Schrödinger equation. J. Phys. A: Math. Theor. **40**(43), 13023 (2007)
21. Q.L. Ning, S.K. Wang, A.P. Luo, Z.B. Lin, Z.C. Luo, W.C. Xu, Bright-dark pulse pair in a figure-eight dispersion-managed passively mode-locked fiber laser. IEEE Photon. J. **4**(5), 1647–1652 (2012)
22. X.L. Li, S.M. Zhang, Y.C. Meng, Y.P. Hao, Harmonic mode locking counterparts of dark pulse and dark-bright pulse pairs. Opt. Express **21**(7), 8409–8416 (2013)
23. B. Guo, Y. Yao, J.J. Xiao, R.L. Wang, J.Y. Zhang, Topological insulator-assisted dual-wavelength fiber laser delivering versatile pulse patterns. IEEE J. Sel. Top. Quantum Electron. **22**(2), 8–15 (2016)
24. R.W. Zhao, G.R. Li, B.T. Zhang, J.L. He, Multi-wavelength bright-dark pulse pair fiber laser based on rhenium disulfide. Opt. Express **26**(5), 5819–5826 (2018)
25. Y. Zheng, M.X. Wang, R. Zhao, H.N. Zhang, D.H. Liu, D.W. Li, Nonlinear optical absorption properties of zirconium selenide in generating dark soliton and dark-bright soliton pairs. Appl. Opt. **59**(2), 396–404 (2020)
26. K.J. Zhao, H.X. Jia, P. Wang, J.J. Guo, X.S. Xiao, C.X. Yang, Free-running dual-comb fiber laser mode-locked by nonlinear multimode interference. Opt. Lett. **44**(17), 4323–4326 (2019)
27. J.T. Wang, Z.K. Jiang, H. Chen, J.R. Li, J.D. Yin, J.Z. Wang, T.C. He, P.G. Yan, S.C. Ruan, High energy soliton pulse generation by a magnetron-sputtering-deposition-grown $MoTe_2$ saturable absorber. Photon. Res. **6**(6), 535–541 (2018)
28. G.W. Chen, W. Li, G.M. Wang, W.F. Zhang, C. Zeng, W. Zhao, Generation of coexisting high-energy pulses in a mode-locked all-fiber laser with a nonlinear multimodal interference technique. Photon. Res. **7**(2), 187–192 (2019)
29. Z.K. Wang, J.K. Chen, T.Y. Zhu, D.N. Wang, F. Gao, Graded index fiber as an all-fiber saturable absorber for large energy conventional soliton and dissipative soliton generation. Photon. Res. **7**(11), 1214 (2019)
30. Z.B. Lin, A.P. Luo, S.K. Wang, H.Y. Wang, W.J. Cao, Z.C. Luo, W.C. Xu, W. Cheng, Generation of dual-wavelength domain-wall rectangular-shape pulses in HNLF-based fiber ring laser. Opt. Laser Technol. **44**(7), 2260–2264 (2012)
31. Y.Y. Qi, M.Y. Liu, N.N. Luan, S. Yang, Z.X. Bai, B.Z. Yan, J. Ding, Y.L. Wang, Z.W. Lv, Recent research progress of nonlinear multimode interference mode-locking technology based on multimode fibers. Infrared Phys. Technol. **121**(8), 104017 (2022)
32. Q.C. Wu, Y.L. Gu, Y. Yao, Y.F. Yang, H.B. Lei, Y.T. Tian, J.J. Tian, B. Guo, Convertible dark pulse and bright pulse fiber ring laser by adjusting the polarization. IEEE Photon. Technol. Lett. **30**(14), 1285–1288 (2018)
33. Z.K. Wang, D.N. Wang, F.Y.L.J. Li, C.L. Zhao, B. Xu, S.Z. Jin, S.Y. Cao, Z.J. Fang, Er-doped mode-locked fiber laser with a hybrid structure of a step-index-graded-index multimode fiber as the saturable absorber. J. Lightwave Technol. **35**(24), 5280–5285 (2017)
34. J.K. Chen, Z.K. Wang, L.J. Li, D.N. Wang, T.Y. Zhu, F. Gao, S.Y. Cao, Z.J. Fang, GIMF-based SA for generation of high pulse energy ultrafast solitons in a mode-locked linear-cavity fiber laser. J. Lightwave Technol. **38**(6), 1480 (2020)
35. Z.P. Dong, J.Q. Lin, H.X. Li, S.J. Li, R.X. Tao, C. Gu, P.J. Yao, L.X. Xu, Generation of mode-locked square-shaped and chair-like pulse based on reverse saturable absorption effect of nonlinear multimode interference. Opt. Express **27**(20), 27610 (2019)
36. J. Gao, F.M. Hu, X.D. Huo, P. Gao, Bright-dark pair in passively mode-locked fiber laser based on graphene. Laser Phys. **24**(8), 085104 (2014)
37. S.G. Fu, X.X. Shang, F. Zhang, Ferromagnetic insulator $Cr_2Ge_2Te_6$ as a modulator for generating near-infrared bright-dark soliton pairs. Appl. Opt. **58**(33), 9217–9223 (2019)
38. H.H. Liu, K.K. Chow, Dark pulse generation in fiber lasers incorporating carbon nanotubes. Opt. Express **22**(24), 29708–29713 (2014)
39. S.J. Fu, G.N. Shi, Q. Sheng, W. Shi, X.S. Zhu, J.Q. Yao, R.A. Norwood, N. Peyghambarian, Dual-wavelength fiber laser operating above 2 μm based on cascaded single-mode-multimode-single-mode fiber structures. Opt. Express **24**(11), 11282–11289 (2016)
40. A. Castillo-Guzman, J.E. Antonio-Lopez, R. Selvas-Aguilar, D.A. May-Arrioja, J. Estudillo-Ayala, P. LiKamWa, Widely tunable erbium-doped fiber laser based on multimode interference effect. Opt. Express **18**(2), 591–597 (2010)
41. S. Chang, Z.K. Wang, D.N. Wang, W.D. Wu, F. Gao, NCF-GIMF device as SA and filter utilized in tunable single- and dual- wavelength Yb-doped mode-locked fiber laser. Opt. Commun. **483**, 126612 (2021)
42. X.R. Zhu, B. Zhang, D.S. Zhao, L.Y. Yang, S.L. Liu, J. Hou, Pulse evolution and multi-pulse state of coherently coupled polarization domain walls in a fiber ring laser. Opt. Express **29**(19), 30558–30566 (2021)
43. X.F. Wang, H.H. Han, D.X. Liu, Generation of bright-dark soliton pairs in mode-locked fiber laser based on molybdenum diselenide. IEEE Access **8**, 160427–160432 (2020)

44. W.S. Mohammed, P.W.E. Smith, X.J. Gu, All-fiber multimode interference bandpass filter. Opt. Lett. **31**(17), 2547–2549 (2006)
45. J.E. Antonio-Lopez, A. Castillo-Guzman, D.A. May-Arrioja, R. Selvas-Aguilar, P. LiKamWa, Tunable multimode-interference bandpass fiber filter. Opt. Lett. **35**(3), 324–326 (2010)